Surface-Dominated Finite-Size Effects in Nanoconfined Superfluid Helium

E. Varga,* C. Undershute, and J. P. Davis†
Department of Physics, University of Alberta, Edmonton, Alberta T6G 2E1, Canada

(Received 16 February 2022; accepted 13 September 2022; published 28 September 2022)

Superfluid ^{4}He (He II) is a widely studied model system for exploring finite-size effects in strongly confined geometries. Here, we study He II confined in millimeter-scale channels of 25 and 50 nm height at high pressures using a nanofluidic Helmholtz resonator. We find that the superfluid density is measurably suppressed in the confined geometry from the transition temperature down to 0.6 K. Importantly, this suppression can be accounted for by rotonlike thermal excitations with an energy gap of 5 K. We show that the surface-bound excitations lead to the previously unexplained lack of finite-size scaling of suppression of the superfluid density.

DOI: 10.1103/PhysRevLett.129.145301

Physical descriptions of condensed matter typically implicitly assume infinite sizes of the studied samples. When surfaces, finite sizes, or restricted geometries are considered, however, novel behaviors often emerge. These range widely across the field of condensed matter, e.g., the quantum hall effect in 2D electron gas [1–3], conducting surface states in topological insulators [4], or the topological phase transition in the 2D XY model [5,6]. Finite-size effects play a significant role in, e.g., technologically relevant quantum dots [7] or properties of nanoparticles [8], where magnetic phase transitions can be strongly altered or even completely suppressed compared to the bulk material [9] or novel collective behaviors can emerge [10,11]. Similarly, in superfluid ^{3}He, surface scattering of Cooper pairs can lead to stabilization of novel superfluid phases [12,13].

Finite-size effects become especially important near phase transitions, where the coherence length diverges [14]. The superfluid phase transition in ^{4}He is one of the most closely studied model systems thanks to the high achievable purity of the medium and relative lack of parasitic effects due shape or interaction with confining walls [15]. Indeed, the most accurate experimental determination of a critical exponent occurred in ^{4}He in a microgravity environment [15]. A detailed understanding of the superfluid transition in ^{4}He is not only useful for tests of modern phase transition theories [15], but also for systems in the same universality class [16].

Because of the ability of superfluid helium (He II) to easily flow in most strongly confined systems, the superfluid transition is a popular model system for the study of finite-size effects near the phase transition. The superfluid order parameter is the macroscopic wave function Ψ, related to the superfluid density as $\rho_s = |\Psi|^2$ [17], which vanishes at the walls [18]. This results in suppression of superfluid density in confined geometries, which, for 2D crossover, is expected [14] to follow

$$\frac{\rho_{sc}}{\rho} = \frac{\rho_{sb}}{\rho}[1 - X(lt^{\nu})], \tag{1}$$

where X is a universal function, ρ is the total density, ρ_{sc} and ρ_{sb} are the superfluid densities in the confined geometry and bulk, respectively, $t = 1 - T/T_\lambda$ is the reduced temperature (T_λ is the bulk transition temperature), $l = D/\xi_0$ is the reduced system size with D the thickness of the slab, ξ_0 the low-temperature coherence length, and $\nu \approx 0.67$ is the correlation length critical exponent.

For He II in the 2D limit, as the critical temperature T_c is approached, the superfluid density vanishes discontinuously [19] at the Kosterlitz-Thouless (KT) transition [5,6,20]. The KT transition was tested to a high degree of accuracy [21], however, the scaling behavior given by (1), is not observed experimentally and the reason for the breakdown is not known [14,22–24]. Breakdown of finite-size scaling was also observed in thermal resistivity [25]. This is in contrast with good agreement of finite-size scaling of the specific heat above T_λ [25–27]. Note that the scaling near the phase transition in 3D and 2D is connected via hyperscaling relations [15], anomalous behavior in He II thus requires close attention.

Here, we observe the suppression of superfluid density in fully confined helium slabs with 25 and 50 nm confinements probed using an on-chip nanofluidic Helmholtz resonance, where tuning the bulk excitation spectrum, coherence length, and the transition temperature is possible by changing the pressure. We observe the suppression for temperatures of 0.6 K to T_λ due to rotonlike excitation with energy gap of 5 K (independent of confinement or pressure) that is localized near the walls. We find that the suppression of the superfluid density at different confinements and pressures, which, notably, does not follow finite-size scaling (1), can be fully accounted for by pressure and confinement dependence of the roton wave vector. The helium slabs exhibit the KT transition, which indicates that the coherence length reaches

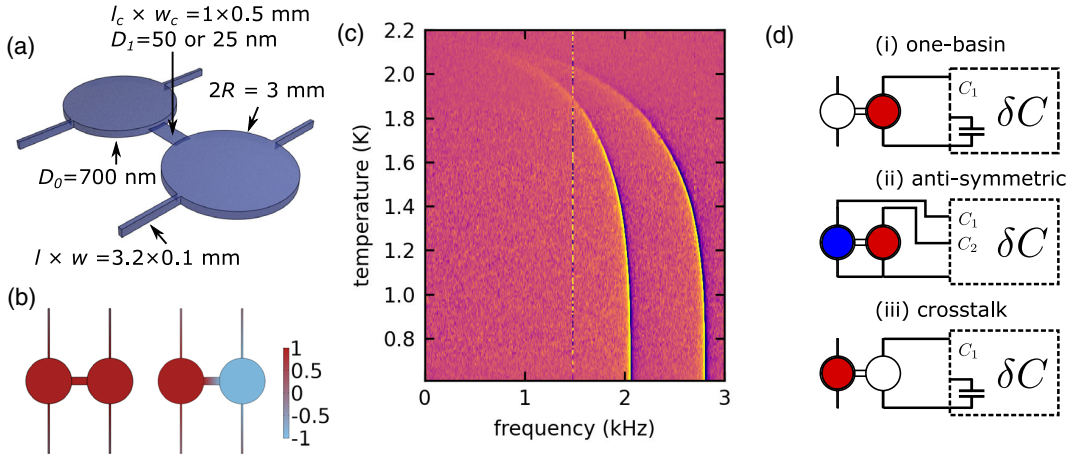

FIG. 1. (a) The confined volume of the nanofluidic Helmholtz resonator. The two circular basins are connected to a pressurized ^{4}He bath via four inlet channels and are interconnected via the strongly confined central channel (see Ref. [32] for AFM images). The basins form parallel plate capacitors (electrodes not shown) used for both sensing and forcing the Helmholtz modes. (b) Pressure amplitude of the two Helmholtz modes used in the study. Note that the fundamental (symmetric) mode shows zero pressure gradient across the strongly confined channel making only the second (antisymmetric) mode sensitive to the superfluid density in the strong confinement. (c) Temperature dependence of the two modes for 50 nm central channel confinement and $P \approx 1$ bar, measured with the one-basin protocol. (d) The three measurement protocols (see Ref. [32] for more detailed description). The "δC" box represents a bridge circuit that measures differential capacitance between one of the basins and a reference capacitor [the one-basin (i) and crosstalk (iii)] or between the two basins [the antisymmetric (ii)]. The coloring of the basin indicates the applied electrostatic force driving the Helmholtz mode: white—not forced, red—forced, blue—forced with a 180° phase shift.

a significant fraction of the confinement close to the transition [5]. In particular, the nature of the superfluid suppression does not change between high-temperature 2D regime, and the low-temperature 3D regime where the coherence length is much shorter than the slab thickness, showing that the surface excitations, rather than coherence length effects, are the dominant process behind finite-size effects in the studied range of parameters. This resolves the long-standing puzzle of breakdown of finite-size scaling in superfluid ^{4}He.

We measure the superfluid fraction ρ_s/ρ using the fourth sound resonance method [12,28–30]. The fourth sound resonance is set up in a nanofluidic Helmholtz resonator, Figs. 1(a) and 1(b), where He II is confined to a thin volume enclosed by a quartz substrate (see Ref. [30] for fabrication details). Here, the resonator differs from previous designs [12,31] by using two separate circular volumes ("basins," confinement $D_0 \approx 700$ nm) interconnected through a strongly confined central channel (confinement $D_1 \approx 25$ or 50 nm). The nanofluidic volume is connected to a surrounding pressurized bath via four inlets. This geometry supports two Helmholtz modes, whose pressure amplitude is shown in Fig. 1(b), which differ in the relative phase of the pressure oscillating in the two basins. In the fundamental mode (frequency ω_0), the pressure oscillates in the two basins in phase, whereas in the second Helmholtz mode (frequency ω_1) the pressure in the basins oscillates with a 180° phase shift. The temperature dependence of the two modes is shown in Fig. 1(c), where the color indicates the magnitude of one quadrature of the response.

Normalizing by the zero-temperature frequencies $\omega_0(0)$ and $\omega_1(0)$, we get for the superfluid fraction of the bulk (see Supplemental Material [32] for derivation)

$$\frac{\rho_{sb}}{\rho} = \frac{\omega_0^2(T)}{\omega_0^2(0)}, \tag{2}$$

and for the confined channel

$$\frac{\rho_{sc}}{\rho} = \frac{\omega_1^2(T) - \omega_0^2(T)}{\omega_1^2(0) - \omega_0^2(0)}. \tag{3}$$

The above expressions neglect the temperature dependence of the total density, which varies by 0.6% from 0 K to T_λ [37]. Experimentally, the lowest attainable temperature was 0.6 K, which was used in place of the zero-temperature limit (for bulk He II at saturated vapour pressure, $\rho_s/\rho >$ 99.99% at 0.6 K [37]).

Since no measurable deviations from bulk behavior are expected for the 700 nm confinement further than 1 mK from the transition temperature [14,28], we use the superfluid fraction determined using the fundamental mode as an *in situ* thermometer calibrated against the bulk superfluid fraction calculated using the HEPAK data [38]. We drive both resonances sufficiently weakly to avoid turbulent nonlinear response [31].

The helium motion is driven and detected using parallel plate capacitors deposited in the device basins, which are wired in a tuned capacitance bridge circuit allowing sensitive detection of pressure fluctuations inside the basin.

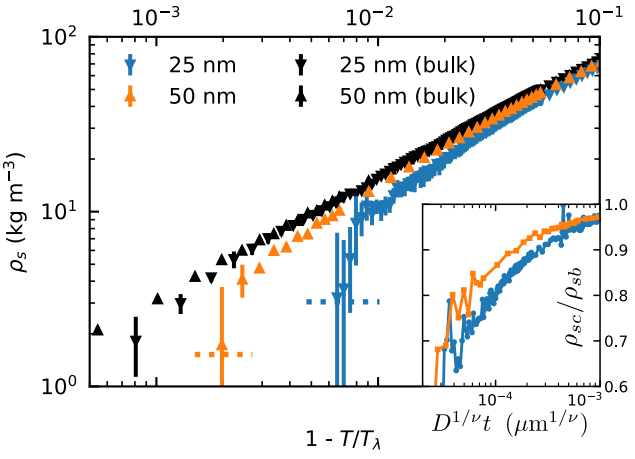

FIG. 2. Superfluid density as a function of reduced temperature in the transition region. The confinement of the central channel of the resonator is shown in the legend. The confined superfluid density is calculated using (3) and the black points show the bulk superfluid density for the corresponding device calculated using (2). Thick dotted horizontal lines indicate the expected KT jump [19]. The error bars are calculated as the standard deviation of a set of measurements with different protocols (i)–(iii) and different drive amplitudes. Inset: ratio of confined and bulk superfluid densities as a function of the scaling variable according to (1). Note that our data do not follow a universal scaling, as has been previously observed [14].

We check the robustness of the measured superfluid densities using three different experimental protocols shown in Fig. 1(d). With the one-basin protocol (i), both modes are excited and detected using only one basin and the two modes show no relative phase shift. With the antisymmetric protocol (ii), only the second Helmholtz mode is driven and observable below the critical temperature T_c of the confined channel. Above T_c, the two basins become decoupled and the fundamental mode frequency is observed, since the mode is degenerate with respect to the phase of the pressure oscillation in the two basins. Finally, the crosstalk protocol (iii) separates the drive and detection. Below T_c we observe both modes with approximately 180° phase shift and above T_c no response is observed (see Ref. [32] for details).

The temperature dependence of the superfluid density in the transition region for the 25 and 50 nm confinements at approximately 1 bar is shown in Fig. 2. Shown by dotted horizontal lines are the expected universal jumps for the two confinements in superfluid density at the KT transition [19], which agree well with our data. The universal jump has been experimentally verified in helium films [39,40], and to a lesser degree also in fully confined geometries [14,29,41,42].

The ratio of the confined and bulk superfluid densities is shown in the inset of Fig. 2 as a function of scaling variable $D^{1/\nu}t$. According to the scaling relation (1), the data should fall on a universal locus. As in previous experiments [14], this is not the case.

Instead, we interpret the suppression of superfluid density as an enhancement of normal fluid density $\rho_n = \rho - \rho_s$ via surface-bound thermal excitations. The density ρ_n is determined by the spectrum of thermal excitations $\varepsilon(k)$ [43], with the dominant contribution above approximately 1 K due to the roton minimum, where

$$\varepsilon^{\mathrm{rot}}(k) = \Delta + \frac{\hbar^2(k-k_0)^2}{2m^*}. \tag{4}$$

Here, $\Delta/k_B \approx 9$ K, $k_0 \approx 2$ Å^{-1}, and $m^* \approx 0.14 m_4$, with m_4 the mass of ^{4}He atom, for bulk helium [44]. The resulting roton contribution to the normal fluid density in two dimensions is [43,45] (in units of mass per area)

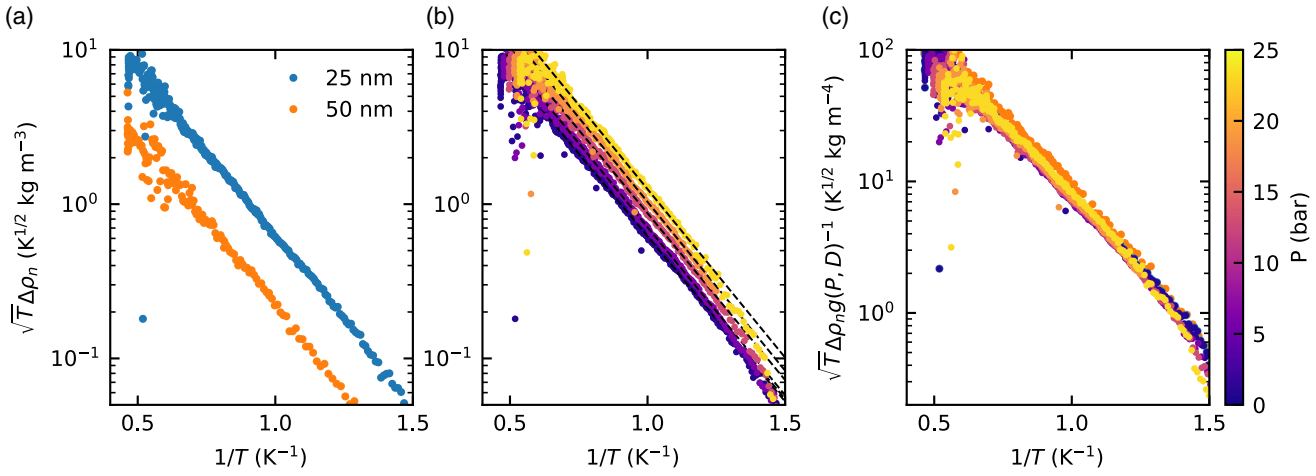

FIG. 3. (a) Normal fluid density enhancement for helium slabs with 25 and 50 nm confinements. (b) Temperature dependence of the normal fluid density enhancement as a function of pressure for 25 nm confinement. The black dashed lines in (a),(b) are linear fits to (5), the roton gap is given by the slope of the line. (c) Data from panels (a) and (b) scaled with $g(P,D) = D^{-1}(1 + P/P^*)[1 + (D^*/D)^3]$ with $P^* = 25$ bar and $D^* = 25$ nm (see text).

$$\rho_n^{2D}(T) = \frac{\hbar k_0^3 m^{*1/2}}{2\sqrt{2\pi k_B T}} \exp\left(-\frac{\Delta}{k_B T}\right). \quad (5)$$

The normal fluid density enhancement, $\Delta\rho_n = \rho_{sc} - \rho_{sb}$, is shown in Fig. 3(a) for the two confinements and pressure $P \approx 1$ bar and in Fig. 3(b) for several $P \in [1, 25]$ bar for the 25 nm confinement as a function of inverse temperature. Plots in Figs. 3(a) and 3(b) are scaled in a manner such that a relation of the type of Eq. (5) appears as a straight line with the slope equal to $-\Delta/k_B$. The temperature dependence in Figs. 3(a) and 3(b) shows excellent agreement with (5) in the full temperature range. Despite the fact that the shown data cover more than an order of magnitude in $\xi(T)/D$, no significant deviation from (5) is observed, which demonstrates that the coherence length does not play a significant role in the observed suppression of the superfluid density.

The roton gap is found to be $\Delta \approx 5$ K, independent of temperature and pressure (see Ref. [32] for additional details), which is in agreement with previous studies with porous materials and helium films, where a temperature dependence of normal fluid density consistent with a roton gap of $\Delta/k_B \approx 4$–6 K was observed [45–47]. Excitations below the bulk roton gap were also observed via inelastic neutron scattering [48,49]. Numerically, it was shown in 2D and quasi-2D helium layers that the roton gap should be significantly reduced compared to the bulk value [50], and it was suggested that this was due to a sharper structure function peak in 2D liquids and backflow enhancement around the roton core [51]. It is also believed that 2D roton excitations exist in the few helium monolayers adjacent to the solidified layers on the substrate [47,52] and only a weak dependence of the reduced gap on the area density (i.e., thickness) is predicted [53,54]. However, the pressure-independent roton gap is in contrast to past observations in bulk [55] and porous media [56,57], suggesting that the behavior of disordered 3D surfaces is more complex.

Adopting the standard bulk-plus-surface approach [14], we assume that the 2D rotons are localized to a thin layer of dense liquid adjacent to the walls. The resulting enhancement of the measured 3D normal fluid density in the confined channel is

$$\Delta\rho_n(T) = \frac{2}{D}\rho_n^{2D}(T). \quad (6)$$

While the measured normal fluid enhancements for two different confinements in Fig. 3(a) clearly differ only by a scaling constant, (6) predicts scaling $\Delta\rho_n \propto D^{-1}$ which does not collapse the data. Similar to the effect of the confinement, a change in pressure only rescales the normal fluid enhancement by a temperature-independent constant, as shown in Fig. 3(b) [see Ref. [32] for pressure dependence of the prefactor in (5)]. Numerical calculations have shown [54] that the 2D roton wave vector k_0 depends on the layer density approximately linearly (we neglect the weak variation of the gap with density [53,54]). Assuming that the density near the wall changes linearly with bulk pressure we can write $k_0(P) = k_P' + k_P'' P$. Retaining only the first order in P, the normal fluid enhancement should scale as $\Delta\rho_n \propto (1 + P/P^*)$, which is found to collapse the data well with $P^* \approx 25$ bar. In this light, confinement dependence can be interpreted as a decrease in density in the boundary region as the separation between the walls increases. Indeed, the pressure at distance z from the wall, outside of the first few solidified layers, varies approximately as $P(z) = P + \alpha/z^3$, where P is the bulk pressure and α depends on the substrate [45,58]. This results in $k_0(D) \approx k_D' + k_D'' D^{-3}$ and $\Delta\rho_n \propto [1 + (D^*/D)^3]D^{-1}$, which does collapse the data for $D^* \approx 25$ nm. The overall confinement and pressure dependence can thus be described as $\Delta\rho_n \propto g(P, D)$ with $g(P, D) = D^{-1}(1 + P/P^*)[1 + (D^*/D)^3]$, which is shown in Fig. 3(c). Since only two confinements are presently available, different relations could equally well describe the data, such as $k_0 \propto D^{-1/6}$ or many others. The scaling with $g(P, D)$ is appealing, however, since it describes pressure and confinement dependence in a unified way, as variation of the fluid density close to the wall.

The exact understanding of the roton behavior in confined slab geometry (e.g., calculation of D^* and P^*) will require numerical calculations of the excitation spectrum for confinements in the range of tens of nanometers, which are within reach of present-day computational resources [59–61]. Nevertheless, the important observation stemming from the present data is that the suppression of superfluidity in 2D confined geometries is dominated by surface excitations, specifically 2D rotons, rather than coherence-length effects as was previously assumed [14]. Even a relatively weak dependence of the roton wave vector on the confinement is a natural explanation of the breakdown of finite-size scaling in confined thin slabs of superfluid ^{4}He. Interestingly, since the growth of the coherence length near T_λ is terminated by the KT transition (or the smallest dimension of the system itself), it is questionable whether a regime of coherence length scaling is ever obtained in real systems. Finally, we also note that the breakdown of scaling due to surface effects was considered also in Ref. [23], although the 2D roton was not identified and the inclusion of the wall attraction on T_λ leads to even greater discrepancy with the experiment [62,63].

In conclusion, using a nanofluidic Helmholtz resonator capable of *in situ* comparison of bulklike and strongly confined behavior of superfluid helium we have shown that the dominant mechanism of suppression of the superfluid density in planar confined geometry are rotonlike quasiparticles with an energy gap of 5 K localized near the wall. This appears to be the dominant mechanism of ρ_s suppression for both 25 and 50 nm confinements for a wide range of pressure and temperature, up to only a few millikelvin below T_λ. A relatively weak dependence of the roton minimum on the confinement naturally explains

the lack of coherence-length scaling which was a long-standing unresolved puzzle [14].

Finite-size effects in confined superfluid helium remain an area of active research [14,24,41,64,65] due, in part, to the ability of modern nanofabrication methods to confine liquid helium to precisely engineered geometries. The general assumption that the confining walls provide simply a termination for the macroscopic wave function [14] is shown to be incomplete. Surface-bound excitations have a strong effect on the dynamics of the confined superfluid, which will likely play a role in future precision tests of modern phase transition theories [15] or novel quantum applications of thin helium layers [66,67].

This work was supported by the University of Alberta; the Natural Sciences and Engineering Research Council, Canada (Grants No. RGPIN-2016-04523 and No. RGPIN-2022-03078); and the Alberta Quantum Major Innovation Fund. C. U. acknowledges support from the University of Alberta Department of Physics SUPRE program.

*ev@ualberta.ca
†jdavis@ualberta.ca

[1] H. L. Stormer, D. C. Tsui, and A. C. Gossard, The fractional quantum Hall effect, Rev. Mod. Phys. **71**, S298 (1999).
[2] T. H. Hansson, M. Hermanns, S. H. Simon, and S. F. Viefers, Quantum Hall physics: Hierarchies and conformal field theory techniques, Rev. Mod. Phys. **89**, 025005 (2017).
[3] K. von Klitzing, T. Chakraborty, P. Kim, V. Madhavan, X. Dai, J. McIver, Y. Tokura, L. Savary, D. Smirnova, A. M. Rey, C. Felser, J. Gooth, and X. Qi, 40 years of the quantum Hall effect, Nat. Rev. Phys. **2**, 397 (2020).
[4] M. Z. Hasan and C. L. Kane, Colloquium: Topological insulators, Rev. Mod. Phys. **82**, 3045 (2010).
[5] J. M. Kosterlitz and D. J. Thouless, Long range order and metastability in two dimensional solids and superfluids. (Application of dislocation theory), J. Phys. C **5**, L124 (1972).
[6] J. M. Kosterlitz and D. J. Thouless, Ordering, metastability and phase transitions in two-dimensional systems, J. Phys. C **6**, 1181 (1973).
[7] P. Lodahl, S. Mahmoodian, and S. Stobbe, Interfacing single photons and single quantum dots with photonic nanostructures, Rev. Mod. Phys. **87**, 347 (2015).
[8] Q. A. Pankhurst, J. Connolly, S. K. Jones, and J. Dobson, Applications of magnetic nanoparticles in biomedicine, J. Phys. D **36**, R167 (2003).
[9] D. Kubániová, L. Kubíčková, T. Kmječ, K. Závěta, D. Nižňanský, P. Brázda, M. Klementová, and J. Kohout, Hematite: Morin temperature of nanoparticles with different size, J. Magn. Magn. Mater. **475**, 611 (2019).
[10] W. P. Halperin, Quantum size effects in metal particles, Rev. Mod. Phys. **58**, 533 (1986).
[11] X. Batlle and A. Labarta, Finite-size effects in fine particles: Magnetic and transport properties, J. Phys. D **35**, 201 (2002).
[12] A. J. Shook, V. Vadakkumbatt, P. Senarath Yapa, C. Doolin, R. Boyack, P. H. Kim, G. G. Popowich, F. Souris, H. Christani, J. Maciejko, and J. P. Davis, Stabilized Pair Density Wave via Nanoscale Confinement of Superfluid ^{3}He, Phys. Rev. Lett. **124**, 015301 (2020).
[13] P. S. Yapa, R. Boyack, and J. Maciejko, Triangular Pair Density Wave in Confined Superfluid ^{3}He, Phys. Rev. Lett. **128**, 015301 (2022).
[14] F. M. Gasparini, M. O. Kimball, K. P. Mooney, and M. Diaz-Avila, Finite-size scaling of ^{4}He at the superfluid transition, Rev. Mod. Phys. **80**, 1009 (2008).
[15] M. Barmatz, I. Hahn, J. A. Lipa, and R. V. Duncan, Critical phenomena in microgravity: Past, present, and future, Rev. Mod. Phys. **79**, 1 (2007).
[16] H. Nishimori and G. Ortiz, *Elements of Phase Transitions and Critical Phenomena*, Oxford Graduate Texts (Oxford University Press, Oxford, 2010).
[17] D. R. Tilley and J. Tilley, *Superfluidity and Superconductivity*, 3rd ed. (IOP Publishing, Bristol, 1990).
[18] M. J. Lea, D. S. Spencer, and P. Fozooni, Healing length near the λ point in liquid helium, Phys. Rev. B **39**, 6527 (1989).
[19] D. R. Nelson and J. M. Kosterlitz, Universal Jump in the Superfluid Density of Two-Dimensional Superfluids, Phys. Rev. Lett. **39**, 1201 (1977).
[20] V. L. Berezinski, Destruction of long-range order in one-dimensional and two-dimensional systems having a continuous symmetry group I. Classical systems, Zh. Eksp. Teor. Fiz. **59**, 907 (1971), http://www.jetp.ras.ru/cgi-bin/e/index/r/59/3/p907?a=list.
[21] J. D. Reppy, Superfluid helium in porous media, J. Low Temp. Phys. **87**, 205 (1992).
[22] M. O. Kimball and F. M. Gasparini, Superfluid Fraction of ^{3}He-^{4}He Mixtures Confined at 0.0483 μm between Silicon Wafers, Phys. Rev. Lett. **86**, 1558 (2001).
[23] F. M. Gasparini, M. O. Kimball, and K. P. Mooney, The superfluid transition of ^{4}He, a test case for finite-size scaling at a second-order phase transition, J. Phys. Condens. Matter **13**, 4871 (2001).
[24] F. M. Gasparini, Confined ^{4}He near T_λ: Scaling and giant proximity effects, J. Low Temp. Phys. **205**, 183 (2021).
[25] D. Murphy, E. Genio, G. Ahlers, F. Liu, and Y. Liu, Finite-Size Scaling and Universality of the Thermal Resistivity of Liquid ^{4}He near T_λ, Phys. Rev. Lett. **90**, 025301 (2003).
[26] M. O. Kimball, K. P. Mooney, and F. M. Gasparini, Three-Dimensional Critical Behavior with 2D, 1D, and 0D Dimensionality Crossover: Surface and Edge Specific Heats, Phys. Rev. Lett. **92**, 115301 (2004).
[27] M. O. Kimball and F. M. Gasparini, Universality and Finite-Size Scaling of the Specific Heat of ^{3}He-^{4}He Mixtures, Phys. Rev. Lett. **95**, 165701 (2005).
[28] X. Rojas and J. P. Davis, Superfluid nanomechanical resonator for quantum nanofluidics, Phys. Rev. B **91**, 024503 (2015).
[29] S. R. D. Thomson, J. K. Perron, and F. M. Gasparini, Long-distance correlation-length effects and hydrodynamics of ^{4}He films in a Corbino geometry, Phys. Rev. B **94**, 094520 (2016).
[30] F. Souris, X. Rojas, P. H. Kim, and J. P. Davis, Ultralow-Dissipation Superfluid Micromechanical Resonator, Phys. Rev. Appl. **7**, 044008 (2017).

[31] E. Varga, V. Vadakkumbatt, A. J. Shook, P. H. Kim, and J. P. Davis, Observation of Bistable Turbulence in Quasi-Two-Dimensional Superflow, Phys. Rev. Lett. **125**, 025301 (2020).

[32] See Supplemental Material at http://link.aps.org/supplemental/10.1103/PhysRevLett.129.145301 for the derivation of the Helmholtz resonances frequencies, details on the electrical circuit used in the experiment, AFM characterization of the confined flow channel, and additional data showing pressure dependence of the roton gap, and which includes Refs. [33–36].

[33] E. Varga and J. P. Davis, Electromechanical feedback control of nanoscale superflow, New J. Phys. **23**, 113041 (2021).

[34] B. Efron, Nonparametric estimates of standard error: The jackknife, the bootstrap and other methods, Biometrika **68**, 589 (1981).

[35] E. Krotscheck and T. Lichtenegger, Dynamic many-body theory: Dynamic structure factor of two-dimensional liquid ^{4}He, J. Low Temp. Phys. **178**, 61 (2015).

[36] J. Bossy, J. Ollivier, and H. R. Glyde, Phonons, rotons, and localized Bose-Einstein condensation in liquid ^{4}He confined in nanoporous FSM-16, Phys. Rev. B **99**, 165425 (2019).

[37] R. J. Donnelly and C. F. Barenghi, The observed properties of liquid helium at the saturated vapor pressure, J. Phys. Chem. Ref. Data **27**, 1217 (1998).

[38] V. D. Arp, R. D. McCarty, and D. G. Friend, Thermophysical properties of Helium-4 from 0.8 to 1500 K with pressures to 2000 MPa, Technical Note (NIST TN) (1998).

[39] D. J. Bishop and J. D. Reppy, Study of the Superfluid Transition in Two-Dimensional ^{4}He Films, Phys. Rev. Lett. **40**, 1727 (1978).

[40] P. Minnhagen, The two-dimensional Coulomb gas, vortex unbinding, and superfluid-superconducting films, Rev. Mod. Phys. **59**, 1001 (1987).

[41] J. K. Perron, M. O. Kimball, K. P. Mooney, and F. M. Gasparini, Coupling and proximity effects in the superfluid transition in ^{4}He dots, Nat. Phys. **6**, 499 (2010).

[42] J. K. Perron and F. M. Gasparini, Critical Point Coupling and Proximity Effects in ^{4}He at the Superfluid Transition, Phys. Rev. Lett. **109**, 035302 (2012).

[43] E. M. Lifshitz and L. D. Landau, *Statistical Physics*, 2nd ed., Course of Theoretical Physics (Pergamon Press, Oxford, 1969), Vol. 5.

[44] H. Godfrin, K. Beauvois, A. Sultan, E. Krotscheck, J. Dawidowski, B. Fåk, and J. Ollivier, Dispersion relation of Landau elementary excitations and thermodynamic properties of superfluid ^{4}He, Phys. Rev. B **103**, 104516 (2021).

[45] M. Chester and L. Eytel, Some calculations regarding the characteristic length for superfluidity in liquid helium, Phys. Rev. B **13**, 1069 (1976).

[46] C. W. Kiewiet, H. E. Hall, and J. D. Reppy, Superfluid Density in Porous Vycor Glass, Phys. Rev. Lett. **35**, 1286 (1975).

[47] D. J. Bishop, J. E. Berthold, J. M. Parpia, and J. D. Reppy, Superfluid density of thin ^{4}He films adsorbed in porous Vycor glass, Phys. Rev. B **24**, 5047 (1981).

[48] B. E. Clements, J. L. Epstein, E. Krotscheck, and M. Saarela, Structure of boson quantum films, Phys. Rev. B **48**, 7450 (1993).

[49] B. E. Clements, H. Godfrin, E. Krotscheck, H. J. Lauter, P. Leiderer, V. Passiouk, and C. J. Tymczak, Excitations in a thin liquid ^{4}He film from inelastic neutron scattering, Phys. Rev. B **53**, 12242 (1996).

[50] T. C. Padmore, Two-Dimensional Rotons, Phys. Rev. Lett. **32**, 826 (1974).

[51] W. Götze and M. Lücke, A comment on rotons in two-dimensional liquid helium II, J. Low Temp. Phys. **25**, 671 (1976).

[52] M. Chester, G. D. L. Webster, E. Webster, and T. Oestereich, Two-Dimensional Interface Excitations: Measurements in ^{3}He-^{4}He Mixtures, Phys. Rev. Lett. **45**, 464 (1980).

[53] V. Apaja and E. Krotscheck, Layer- and Bulk-Roton Excitations of ^{4}He in Porous Media, Phys. Rev. Lett. **91**, 225302 (2003).

[54] F. Arrigoni, E. Vitali, D. E. Galli, and L. Reatto, Excitation spectrum in two-dimensional superfluid ^{4}He, J. Low Temp. Phys. **39**, 793 (2013).

[55] H. Godfrin, M. Meschke, H.-J. Lauter, A. Sultan, H. M. Böhm, E. Krotscheck, and M. Panholzer, Observation of a roton collective mode in a two-dimensional Fermi liquid, Nature (London) **483**, 576 (2012).

[56] K. Yamamoto, Y. Shibayama, and K. Shirahama, Thermodynamic Evidence for Nanoscale Bose-Einstein Condensation in ^{4}He Confined in Nanoporous Media, Phys. Rev. Lett. **100**, 195301 (2008).

[57] J. Bossy, J. Ollivier, H. Schober, and H. R. Glyde, Phonon-roton modes in liquid ^{4}He coincide with Bose-Einstein condensation, Europhys. Lett. **98**, 56008 (2012).

[58] J. S. Brooks, B. B. Sabo, P. C. Schubert, and W. Zimmermann, Helmholtz-resonator measurements of the superfluid density of liquid ^{4}He in submicrometer-diameter channels, Phys. Rev. B **19**, 4524 (1979).

[59] V. Apaja and E. Krotscheck, Layered ^{4}He and ^{3}He-^{4}He mixture between two surfaces, Phys. Rev. B **64**, 134503 (2001).

[60] V. Apaja and E. Krotscheck, Excitations in confined helium, Phys. Rev. B **67**, 184304 (2003).

[61] E. Krotscheck and V. Apaja, Dynamics of confined quantum fluids, Eur. Phys. J. Special Topics **141**, 83 (2007).

[62] X. F. Wang, I. Rhee, and F. M. Gasparini, Calculation of van der Waals effects on correlation-length scaling near, Physica (Amsterdam) **165–166B**, 593 (1990).

[63] K. P. Mooney and F. M. Gasparini, Van der Waals effects at the superfluid transition of confined ^{4}Helium, J. Low Temp. Phys. **126**, 247 (2002).

[64] B. Kulchytskyy, G. Gervais, and A. Del Maestro, Local superfluidity at the nanoscale, Phys. Rev. B **88**, 064512 (2013).

[65] A. Del Maestro and B. Rosenow, Dissipation in mesoscale superfluids, Phys. Rev. B **95**, 140507(R) (2017).

[66] X. He, G. I. Harris, C. G. Baker, A. Sawadsky, Y. L. Sfendla, Y. P. Sachkou, S. Forstner, and W. P. Bowen, Strong optical coupling through superfluid Brillouin lasing, Nat. Phys. **16**, 417 (2020).

[67] Y. L. Sfendla, C. G. Baker, G. I. Harris, L. Tian, R. A. Harrison, and W. P. Bowen, Extreme quantum nonlinearity in superfluid thin-film surface waves, npj Quantum Inf. **7**, 62 (2021).